Theory of dislocation-solute atom interactions in solid solutions and related nonlinear anelasticity

G. Gremaud and S. Kustov*
Institut de Génie Atomique, Ecole Polytechnique Fédérale de Lausanne, CH-1015 Lausanne, Switzerland
(Received 7 December 1998; revised manuscript received 16 April 1999)

A theory for dislocation-solute atom interactions in solid solutions has been developed which allows one to calculate the nonlinear dislocation strain-amplitude-dependent internal friction. The suggested model accounts for different modes of dislocation-solute atom interactions: (i) Solute atoms distributed in the dislocation glide plane interact with the dislocation core and represent short-range obstacles for the dislocation motion; (ii) Solute atoms situated away from the dislocation glide plane create relatively weak long-range elastic stress fields, also impeding dislocation motion. We assume that dislocations move in a two-component system of obstacles which differ with respect to the thermodynamics of dislocation–point-defect interactions. Namely, dislocations overcome short-range obstacles under the combined action of applied stress and thermal energy, whereas relatively weak long-range obstacles are surmounted athermally. The model predicts a complicated multistage behavior of the nonlinear internal friction in the strain amplitude–temperature–solute concentration domain, which is in excellent agreement with recent experimental data. [S0163-1829(99)10033-X]

I. INTRODUCTION

It is generally agreed upon that dislocation-related strain-amplitude-dependent internal friction (ADIF) in crystals, at moderate stress amplitudes (i.e., well below the yield stress of a crystal), is due to the reversible oscillatory motion of dislocations over stress fields of lattice point defects,[1] although, under certain circumstances, nonlinear anelasticity may originate from intrinsic properties of dislocations[2] or dislocation-dislocation interactions.[3,4] Despite the fact that numerous theories of the internal friction (IF) due to dislocation–point-defect interactions have been developed, a theoretical background for several important issues is still lacking.[5] Among those issues are the problem of the low-strain amplitude IF background in pure metals and solid solutions in the low-frequency range,[6] the peaking effect during irradiation of crystals,[7] and the low-temperature athermal ADIF in crystals with different crystallographic structure.[8,9]

Existing theories of the ADIF usually consider the thermally activated breakaway or continuous pinning and depinning of dislocations from the lattice defects, distributed (homogeneously or heterogeneously) in the dislocation glide plane. Traditionally, in the case of dislocation motion in a two-component system of obstacles, it has been inferred that solute atoms distributed in dislocation glide planes represent weak and short-range obstacles which dislocations overcome with the assistance of thermal fluctuations, whereas forest dislocations create strong obstacles.[10] An approach has been suggested in Ref. 5 to account for the aforementioned unsolved problems. It has been assumed that for an adequate description of the dislocation motion in the anelastic range, dislocation interactions with elastic stress fields of lattice defects distributed in the bulk of a crystal, should be considered as well as short-range interactions with defects distributed in the dislocation glide plane. Thus, even in the simplest case of immobile solute atoms of the same nature (or point obstacles for the dislocation motion) homogeneously distributed in the bulk of a crystal, two different modes of dislocation interactions with those obstacles should be taken into account. Recently, a detailed experimental investigation of the ADIF in solid solutions of the CuNi system has been performed.[9] In the present paper we suggest a quantitative model for the ADIF in solid solutions and compare its predictions with available experimental data.

II. MODEL

A. Elementary dislocation–single foreign atom interactions

Dislocation–foreign atom interactions originate from various mechanisms: atomic size misfit, modulus effect, or ''electrostatic'' effect when a foreign atom has a valence different from that of the host atom.[11] Consider, for simplicity, the case of atomic size misfit, when a substitutional solute atom is a dilatation center with spherical symmetry.[12] If the foreign atom is situated at a distance z from the glide plane of an edge dislocation with the Burgers vector along the x axis (Fig. 1), the interaction force between the dislocation gliding in the x direction and the foreign atom is[11]

$$F(x)=\frac{\mu b\,\delta V^{\infty}}{\pi z^2}\,\frac{2x/z}{(1+x^2/z^2)^2}=F_{\max}\varphi(x/z), \qquad (1)$$

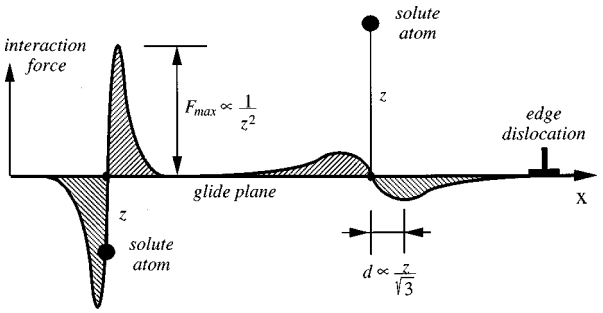

FIG. 1. Force-distance profiles for dislocation-solute atom interactions, in the case of atomic size misfit and edge dislocation, for different relative position and distance between dislocation and solute atom.

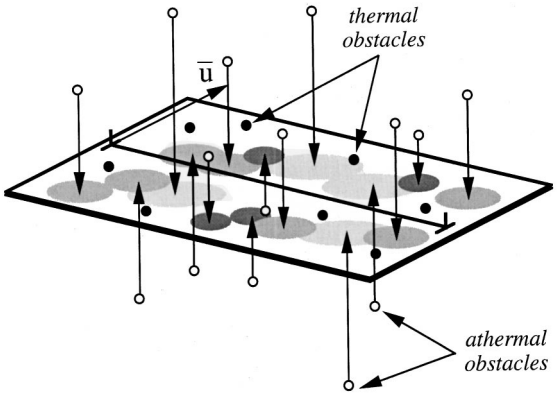

FIG. 2. Schematic representation of a dislocation, gliding with the average displacement $\bar{u}$ in stress fields of solute atoms distributed in the bulk of a crystal. Small full circles represent solute atoms in a few atomic planes, adjacent to the dislocation glide plane. They create strong short-range obstacles in the dislocation glide plane, which can be surmounted with the assistance of thermal fluctuations. Open circles show solute atoms, situated away from the dislocation glide plane. Large gray symbols on the glide plane represent long-range athermal stress fields due to these atoms. The range of interaction and the maximum interaction force, as represented by the size and darkness of symbols, depend on the spacing between the atom and glide plane.

where δV^{∞} is the change of the volume of the unstrained lattice by the substitution for a solute atom, μ is the shear modulus, b is the Burgers vector magnitude. Profiles (1) are plotted in Fig. 1 for two different spacings z between the solute atoms and dislocation glide plane. The maximum interaction force between the dislocation and foreign atom depends strongly on the spacing z:

$$F_{\max} \propto 1/z^2. \tag{2}$$

For the case of modulus effect,[11] one has

$$F_{\max} \propto 1/z^3. \tag{3}$$

The range of the dislocation-solute atom interaction increases with the spacing z. For example, for the atomic size misfit, Eq. (2), the maximum of the interaction force along the gliding direction x occurs at a distance $d=z/\sqrt{3}$ from the atom's projection on the glide plane. Thus, solute atoms in the slip plane or in a few adjacent atomic planes interact with the dislocation on a short range, comparable with the Burgers vector magnitude b. Solute atoms situated away from the glide plane give rise to relatively small but long-range stresses. The former case corresponds to localized, and the latter to diffuse forces, exerted on the dislocation.[13] This situation can be represented schematically by Fig. 2, where full and open spheres represent foreign atoms, distributed in the vicinity and away from the dislocation glide plane, respectively. The atoms, situated away from the glide plane, create weak but long-range stresses in the glide plane, as shown by gray symbols in Fig. 2. The diffuse forces are considered as internal stresses, slowly varying in space (compared to the Burgers vector magnitude b), with a mean amplitude σ_i.[13,14]

The present model is based on an assumption that dislocations overcome these two types of obstacles in essentially

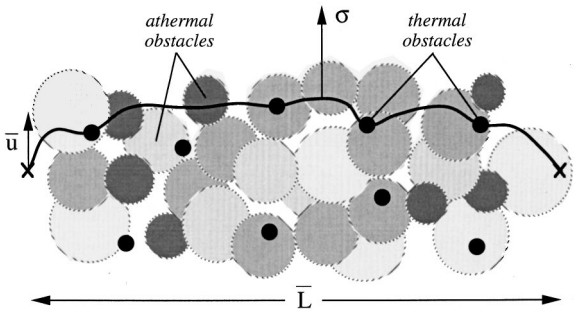

FIG. 3. The model for the dislocation motion with an average displacement $\bar{u}$ in the field of localized thermally activated obstacles (small full circles) and diffuse long-range athermal stress fields (gray large circles) under the action of an applied stress σ. Crosses represent impenetrable pinning points.

different ways. Dislocations overcome localized forces under the combined action of the applied stress and thermal fluctuations. Relatively weak but long-range diffuse forces are surmounted athermally. We believe that weak long-range obstacles are not intrinsically athermal. Rather, the waiting time for a fluctuation becomes very long for long-range obstacles, even if the activation energy is relatively low. We suppose that this is due to a low attack frequency for overcoming long-range obstacles.[15] This problem deserves special attention and is beyond the scope of the present work. In what follows we will accept the athermal nature of long-range obstacles as a hypothesis and will verify its validity comparing experimental results with predictions of the model.

Schematically, the simultaneous motion of a dislocation with an average displacement $\bar{u}$ under applied stress σ in the two-component system of obstacles can be represented by Fig. 3. We also introduce strong impenetrable obstacles, for instance, due to the nodes of the dislocation network, at a larger space scale $\bar{L}$, as indicated by crosses in Fig. 3. We will consider first (separately) interactions of dislocations with these three types of obstacles.

B. Basic ingredients of the model

1. Motion of a dislocation over athermal diffuse forces

The interaction force between a dislocation and a solute atom situated away from the dislocation glide plane depends on the distance between the solute atom and glide plane [Eq. (2) in the case of atomic size misfit]. Therefore, we introduce the distribution function $n(f)$ of the number of athermal forces per unit area of the glide plane, which is proportional to the atomic concentration C of the solute atoms and is dependent on their distribution in the bulk of a crystal:

$$n(f)df = A\frac{C}{f^{\beta}}df,$$

$$f < f_{\max}, \tag{4}$$

where A is a normalization constant, β is a parameter dependent on the distribution of solute atoms in the bulk and the nature of dislocation-solute atom interaction. This distribu-

tion is limited by the maximum value of the interaction force $f_{\max}$ for which dislocation-point obstacle interaction is still athermal.

Consider, for example, the case of size misfit and random solid solution, i.e., the homogeneous volume distribution of solute atoms. The number $n(z)dz$ of solute atoms per unit area of the dislocation glide plane, situated on both sides of the dislocation glide plane at a distance z in the range dz is

$$n(z)dz = 2\frac{C}{a^3}dz, \tag{5}$$

where a is the lattice parameter. Since from Eq. (2)

$$dz \propto \frac{1}{f^{3/2}}df, \tag{6}$$

one obtains from Eqs. (5) and (6) for the atomic size misfit and homogeneous solid solution

$$n(f)df = AC\frac{1}{f^{3/2}}df, \tag{7}$$

i.e., the parameter β in Eq. (4) becomes equal to 3/2. For the modulus effect one obtains from Eqs. (3), (5), and (4): $\beta = 4/3$.

The number $N(F)$ of obstacles per unit area of the dislocation glide plane having the maximum interaction force equal or higher than F is given by

$$N(F) = N(f>F) = \int_F^{f_{\max}} n(f)df = A\frac{C}{\beta-1}\left(\frac{1}{F^{\beta-1}} - \frac{1}{f_{\max}^{\beta-1}}\right). \tag{8}$$

In what follows, we suggest using a more convenient approximate form for $N(F)$

$$N(F) = \begin{cases} A\dfrac{C}{\beta-1}\dfrac{1}{F^{\beta-1}} & \text{if } f<f_{\max}, \\ 0 \quad \text{if } f \geqslant f_{\max}. \end{cases} \tag{9}$$

It is well known that in solid solutions the most stable dislocation configuration even in the absence of external stress is a zigzag form,[14,16] shown in Fig. 4(a). The average length of a zigzag along the dislocation line $\overline{l}$ and zigzag amplitude $\overline{d}$ satisfy the condition

$$h^2 = \overline{dl}, \tag{10}$$

where h is the average obstacle spacing in the glide plane. Under applied stress, the dislocation has a configuration, depicted in Fig. 4(b), with the angles α_1 and α_2

$$\alpha_1 \cong \overline{d}/\overline{l} = (h/\overline{l})^2, \qquad \alpha_2 \cong \frac{b\overline{l}\sigma}{2\gamma}, \tag{11}$$

where $\gamma = \mu b^2$ is the line tension.

The average pinning force, acting between the dislocation and point obstacle is given by

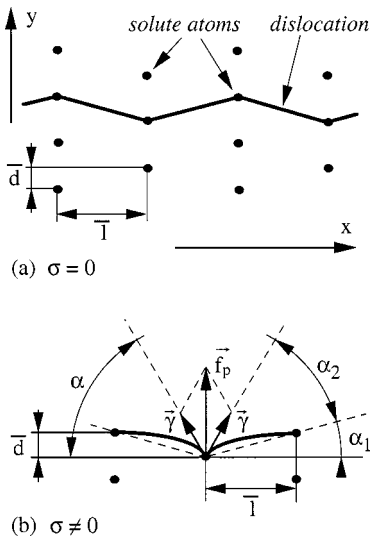

FIG. 4. Zigzag configuration of a dislocation in a random solid solution (a) and bowing out of segments of the zigzagged dislocation under applied stress (b).

$$f_p \cong 2\gamma(\alpha_1+\alpha_2) \cong 2\gamma\left(\frac{h^2}{\overline{l}^2} + \frac{b\overline{l}\sigma}{2\gamma}\right). \tag{12}$$

Minimization of the average pinning force under condition (10) leads to the well-known dynamic Friedel's distribution[16,17] of $\overline{l}$ and $\overline{d}$:

$$\overline{l} = \left(\frac{4h^2\gamma}{b\sigma}\right)^{1/3}, \qquad \overline{d} = \left(\frac{h^4 b\sigma}{4\gamma}\right)^{1/3}. \tag{13}$$

Substituting $\overline{l}$ from Eq. (13) into Eq. (12) one obtains the average pinning force for Friedel's statistics:

$$f_p = 3(\gamma h^2 b^2/2)^{1/3}\sigma^{2/3}. \tag{14}$$

Let us apply the dynamic Friedel distribution to the motion of a dislocation in the system of athermal obstacles. When obstacles with retention force $f>F$ stop the dislocation, their number per unit area of the glide plane is

$$N(F) = \frac{1}{h^2}. \tag{15}$$

Supposing that the average pinning force f_p is equal to the retention force F sufficient to stop the dislocation under applied stress σ, one obtains from Eqs. (14) and (15)

$$F = 3\left(\frac{\gamma b^2}{2N(F)}\right)^{1/3}\sigma^{2/3}. \tag{16}$$

Substituting $N(F)$ from Eq. (9) into Eq. (16) we deduce the dependence of the retention force on the applied stress:

$$F = \left(\frac{27\gamma b^2(\beta-1)}{2AC}\right)^{1/(4-\beta)}\sigma^{2/(4-\beta)}. \tag{17}$$

Since the average displacement of the dislocation corresponds to the zigzag amplitude, $\overline{u} \cong \overline{d}$, one has from Eqs. (13), (15), (9), and (17)

$$\sigma = BC^{2/\beta}\overline{u}^{(4-\beta)/\beta}, \tag{18}$$

where

$$B = \frac{9^{(1-\beta)/\beta}}{b\gamma}\left(\frac{2A\gamma}{\beta-1}\right)^{2/\beta}$$

is a constant parameter.

For $F \to f_{\max}$, one obtains from Eq. (8) that $N(F) \to 0$, that is, the average displacement of the dislocation is not controlled any more by athermal obstacles. A reasonable estimate of a critical stress σ_{cr1} for the motion of the dislocation in the stress field of athermal obstacles can be deduced from Eq. (17) substituting $F = f_{\max}$:

$$\sigma_{cr1} = E\sqrt{C}, \tag{19}$$

where

$$E = \sqrt{\frac{2A}{27b^2\gamma(\beta-1)}} f_{\max}^{(4-\beta)/2}$$

is a constant parameter.

The stress-anelastic strain dependence and the concentration dependence of the critical stress for the motion of a zigzagged dislocation over athermal diffuse forces can be written finally as

$$\sigma = BC^{(\alpha+1)/2}\overline{u}^{\alpha}, \quad \text{if } \sigma < \sigma_{cr1},$$

$$\sigma_{cr1} = E\sqrt{C} \tag{20}$$

with the exponent α in the power dependence of the dislocation displacement on applied stress

$$\alpha = \frac{4-\beta}{\beta}. \tag{21}$$

Equations (20) are sufficient to determine the component of the internal friction, associated with the dislocation motion over athermal obstacles. We introduce a rheological model for this component of the total anelasticity of solid solutions as a solid friction element with cyclic stress-anelastic strain response as indicated schematically in Fig. 5(a).

2. Motion of a dislocation over localized short-range obstacles

We will consider dislocation motion over the localized short-range obstacles due to solute atoms distributed in a few adjacent atomic planes as continuous thermally activated pinning and depinning of a dislocation line without hard pinning points. We will restrict ourselves to average parameters, without analysis of the statistical problem of finding the relation between single dislocation-solute atom interaction and critical stress for dislocation motion.

Surface density N of short-range obstacles is a function of the solute atom concentration C:

$$N = \varphi C, \tag{22}$$

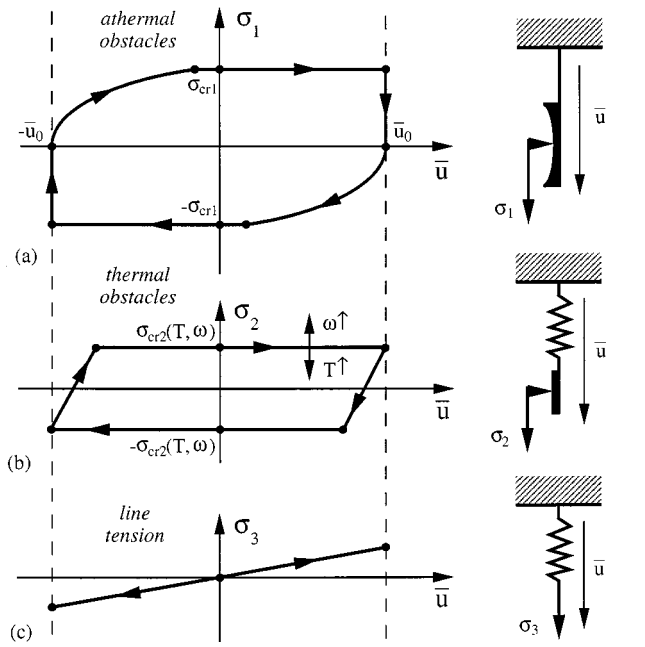

FIG. 5. Rheological models with corresponding stress-anelastic strain hysteresis loops, representing the motion of a dislocation in stress fields of diffuse (a) and localized forces (b), and under the action of line tension between impenetrable pinning points (c).

where φ is a parameter reflecting the distribution of solute atoms in the vicinity of dislocations. This parameter accounts for homogeneous or heterogeneous distribution of solute atoms around dislocations. The former case corresponds to the random solid solution, the latter corresponds for example, to pinning of dislocations due to strain aging. We suggest that, at a stress below the critical stress of dislocation motion, the static Mott statistics[14,18] is applicable. The sum of the line tension energy and the binding energy ΔG_m with solute atom per unit length along the dislocation direction is

$$E_d = (\gamma\sqrt{\overline{l}^2 + \overline{d}^2} - \Delta G_m)/\overline{l}. \tag{23}$$

Minimization of Eq. (23) with Eqs. (10), (15), and (22), and not too large deviations of dislocation from the straight line, gives $\overline{l}$ and $\overline{d}$ in the case of Mott statistics

$$\overline{l} = \left(\frac{2\gamma}{\varphi^2 C^2 \Delta G_m}\right)^{1/3},$$

$$\overline{d} = \left(\frac{\Delta G_m}{2\gamma\varphi C}\right)^{1/3}. \tag{24}$$

One obtains the average pinning force for the Mott statistics by substituting Eq. (24) into Eq. (12):

$$f_p = \left(\frac{2b^3\gamma}{\varphi^2 C^2 \Delta G_m}\right)^{1/3}\sigma + (2\varphi C \Delta G_m \gamma)^{1/3}. \tag{25}$$

Thermally activated depinning should be considered in the case of localized obstacles. Therefore, under oscillatory stress with amplitude σ_0 and circular frequency ω, the critical force of depinning from obstacle F_{cr} (as well as the critical stress σ_{cr2}) becomes frequency and temperature dependent. We will not consider here the existing theoretical

predictions of their temperature and frequency dependence, see for example Ref. 19, and introduce formally the temperature and frequency dependence of the pinning force $F_{cr}(T,\omega)$ and critical stress $\sigma_{cr2}(T,\omega)$. Equation (25) then gives the critical depinning stress

$$\sigma_{cr2}(T,\omega)=\frac{1}{b}\left(\sqrt[3]{\frac{\varphi^2\Delta G_m}{2\gamma}}\sqrt[3]{C^2}F_{cr}(T,\omega)-\varphi C\Delta G_m\right). \tag{26}$$

We account also for the anelastic strain due to the bowing out of dislocation segments between localized obstacles. If $\sigma<\sigma_{cr2}(T,\omega)$, bowing out of dislocation segments is responsible for the following average displacement of the dislocation:

$$\overline{u}=\frac{b\sigma}{12\gamma}\overline{l^2}, \tag{27}$$

where $\overline{l}$ is given by Eq. (24). Finally, the stress-anelastic strain response due to the motion of the dislocation over localized obstacles is given by

$$\sigma=C^{4/3}P\overline{u} \quad \text{if} \quad \sigma<\sigma_{cr2}(T,\omega),$$

$$\sigma_{cr2}(T,\omega)=C^{2/3}Q(T,\omega), \tag{28}$$

where P and Q are parameters, of which Q is temperature and frequency dependent:

$$P=\frac{6}{b}(\sqrt{2\gamma}\varphi^2\Delta G_m)^{2/3},$$

$$Q(T,\omega)\approx\frac{1}{b}\left[\left(\frac{\varphi^2\Delta G_m}{2\gamma}\right)^{1/3}F_{cr}(T,\omega)-\varphi C^{1/3}\Delta G_m\right]. \tag{29}$$

We assumed in Eq. (29) that, as a first approximation, $Q(T,\omega)$ is only temperature and frequency dependent, neglecting weak concentration dependence of its second term.

The rheological model associated with the bowing out and continuous thermally activated pinning and depinning of the dislocation from short-range obstacles is conventionally represented by a solid friction element in a series with an element of elasticity, Fig. 5(b). Figure 5(b) also shows schematically the corresponding cyclic stress–anelastic strain behavior, and the influence of increasing temperature and/or frequency on the critical stress $\sigma_{cr2}(T,\omega)$.

3. Restoring force due to line tension of dislocation between unbreakable pinning points

Finally, account should be taken of the restoring force due to the line tension of a dislocation segment $\overline{L}$ between two unbreakable obstacles. Similar to Eq. (27), the average displacement of the dislocation line is

$$\overline{u}=\frac{b\overline{L^2}}{12\gamma}\sigma. \tag{30}$$

Introducing a new constant parameter $S=12\gamma/b\overline{L^2}$, one obtains from Eq. (30) for the stress due to dislocation line tension between unbreakable pinning points

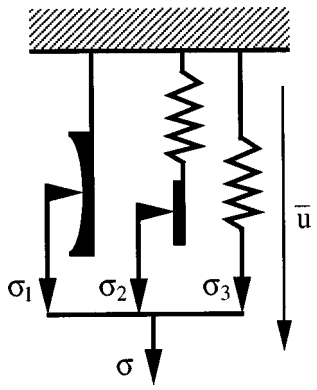

FIG. 6. Rheological model for the motion of a dislocation in solid solution under applied stress σ with the stress components, corresponding to overcoming of diffuse long-range obstacles, σ_1, and localized ones, σ_2, and to the action of the line tension between impenetrable pinners, σ_3.

$$\sigma=S\overline{u}. \tag{31}$$

On the rheological level, Eq. (31) corresponds to an element of elasticity with the appropriate stress-strain behavior, as represented in Fig. 5(c).

C. Rheological model for the nonlinear anelasticity in solid solutions

We have introduced separately three basic ingredients of dislocation anelasticity in solid solutions with their corresponding rheological interpretations. When the dislocation is displaced from its equilibrium position under the action of applied stress, as depicted in Fig. 3, all three types of obstacles, discussed in the previous sections, impede its motion. Therefore, the total applied stress σ is composed of the three components, associated with different mechanisms

$$\sigma=\sigma_1+\sigma_2+\sigma_3, \tag{32}$$

where σ_1, σ_2, σ_3 are the components of the applied stress due to diffuse, localized forces and the line tension due to bowing out of the dislocation between unbreakable pinning points, respectively. We assume that these components are determined by the corresponding Eqs. (20), (28), and (31). Using Eqs. (20), (28), and (31), which define separately each of the mechanisms, in Eq. (32) implies that all three components are assumed to be independent, interrelated only via the magnitude of applied stress. Here we follow the usual approach to treating different components of applied stress as additive, for example, line tension, viscous friction, and inertial term in the case of the oscillating string model. At the rheological level, Eq. (32) can be thought of as a parallel connection of the separate rheological elements. The complete rheological model associated with Eq. (32) with the components defined by Eqs. (20), (28), and (31) is represented in Fig. 6.

III. NUMERICAL SIMULATION. COMPARISON WITH EXPERIMENT

Formally, four different cases are possible, depending on the relationship between the values of the applied stress com-

ponents σ_1, σ_2 and critical stresses $\sigma_{cr1}, \sigma_{cr2}(T,\omega)$:
Low stress amplitudes

$$\sigma_1 < \sigma_{cr1},$$

$$\sigma_2 < \sigma_{cr2}(T,\omega). \tag{33}$$

Intermediate stress amplitudes

$$\sigma_1 = \sigma_{cr1},$$

$$\sigma_2 < \sigma_{cr2}(T,\omega) \tag{34}$$

or

$$\sigma_1 < \sigma_{cr1},$$

$$\sigma_2 = \sigma_{cr2}(T,\omega). \tag{35}$$

High stress amplitudes

$$\sigma_1 = \sigma_{cr1},$$

$$\sigma_2 = \sigma_{cr2}(T,\omega). \tag{36}$$

Despite the simplicity of Eqs. (20), (28), and (31) relating the components σ_1, σ_2, σ_3 to the anelastic strain, a general analytical solution for the dependence $\overline{u}(\sigma)$ does not exist for any of the conditions (33)–(36). In the present work, numerical calculations of the anelastic response have been performed for the periodic applied stress $\sigma(t) = \sigma_0 \sin \omega t$. At this stage it is worthwhile to operate with the macroscopic anelastic strain ε_{an} rather than with the average dislocation displacement. Since anelastic strain is

$$\varepsilon_{an} = \rho b \overline{u}, \tag{37}$$

where ρ is the density of mobile dislocations, all of the previous algebraic manipulations are valid for the anelastic strain. We note now that the anelastic strain rate can be easily derived analytically from Eq. (32) accounting for Eqs. (37), (20), (28), and (31);

$$\dot{\varepsilon}_{an} = \dot{\sigma} \Big/ \left(\alpha B C^{(\alpha+1)/2} \frac{\varepsilon_{an}^{\alpha-1}}{(\rho b)^{\alpha}} + C^{4/3} \frac{P}{\rho b} + \frac{S}{\rho b} \right),$$

$$\dot{\varepsilon}_{an} = \dot{\sigma} \Big/ \left(C^{4/3} \frac{P}{\rho b} + \frac{S}{\rho b} \right),$$

$$\dot{\varepsilon}_{an} = \dot{\sigma} \Big/ \left(\alpha B C^{(\alpha+1)/2} \frac{\varepsilon_{an}^{\alpha-1}}{(\rho b)^{\alpha}} + \frac{S}{\rho b} \right),$$

$$\dot{\varepsilon}_{an} = \rho b \frac{\dot{\sigma}}{S} \tag{38}$$

for all of the conditions (33)–(36), respectively. We introduce dimensionless parameters

$$A_1 = \frac{\alpha B}{S} \left(\frac{E}{S} \right)^{\alpha-1},$$

$$A_2 = \frac{P}{S}, \tag{39}$$

and dimensionless variables

$$a_1 = \frac{\sigma_0}{E} = \sqrt{C} \frac{\sigma_0}{\sigma_{cr1}},$$

$$a_2(T,\omega) = \frac{Q(T,\omega)}{E} = \frac{1}{\sqrt[6]{C}} \frac{\sigma_{cr2}(T,\omega)}{\sigma_{cr1}},$$

$$Y = \left(\frac{\varepsilon_{an}}{\rho b^2} \right) \left(\frac{S}{E\sqrt{C}} \right),$$

$$\Sigma = \frac{\sigma(t)}{\sigma_{cr1}} = \frac{a_1}{\sqrt{C}} \sin \omega t, \tag{40}$$

where a_1 is an independent variable, related to the applied stress amplitude, and Y is proportional to the anelastic strain. Parameter $a_2(T,\omega)$ is associated with the temperature- and frequency-dependent critical stress for the thermally activated depinning of dislocations. The explicit form of the temperature (frequency) dependence of this critical stress has not been discussed in the present work, see Sec. II B 2. Nevertheless, we will consider $a_2(T,\omega)$ as an independent variable, related to the temperature and/or frequency. Equations (38) in dimensionless form are

$$\dot{Y} = \frac{\dot{\Sigma}}{A_1 Y^{\alpha-1} C^{\alpha} + A_2 C^{4/3} + 1},$$

$$\dot{Y} = \frac{\dot{\Sigma}}{A_2 C^{4/3} + 1},$$

$$\dot{Y} = \frac{\dot{\Sigma}}{A_1 Y^{\alpha-1} C^{\alpha} + 1},$$

$$\dot{Y} = \dot{\Sigma} \tag{41}$$

for all of the conditions (33)–(36), respectively.

Two parameters, A_1 and A_2, together with the constant α, determine completely the shape of the stress-anelastic strain hysteresis. Introducing two additional parameters, A_3 and A_4, as

$$A_3 = \frac{\rho b}{JS},$$

$$A_4 = \rho b \frac{E}{S}, \tag{42}$$

where J is the elastic compliance, and recalling that the decrement and modulus defect are

$$\delta_h = \frac{1}{J\sigma_0^2} \oint \varepsilon_{an} d\sigma,$$

$$\frac{\Delta J}{J} = \frac{\varepsilon_{an}|_{\sigma=\sigma_0}}{J\sigma_0}, \tag{43}$$

one obtains from Eqs. (43), (42), and (40)

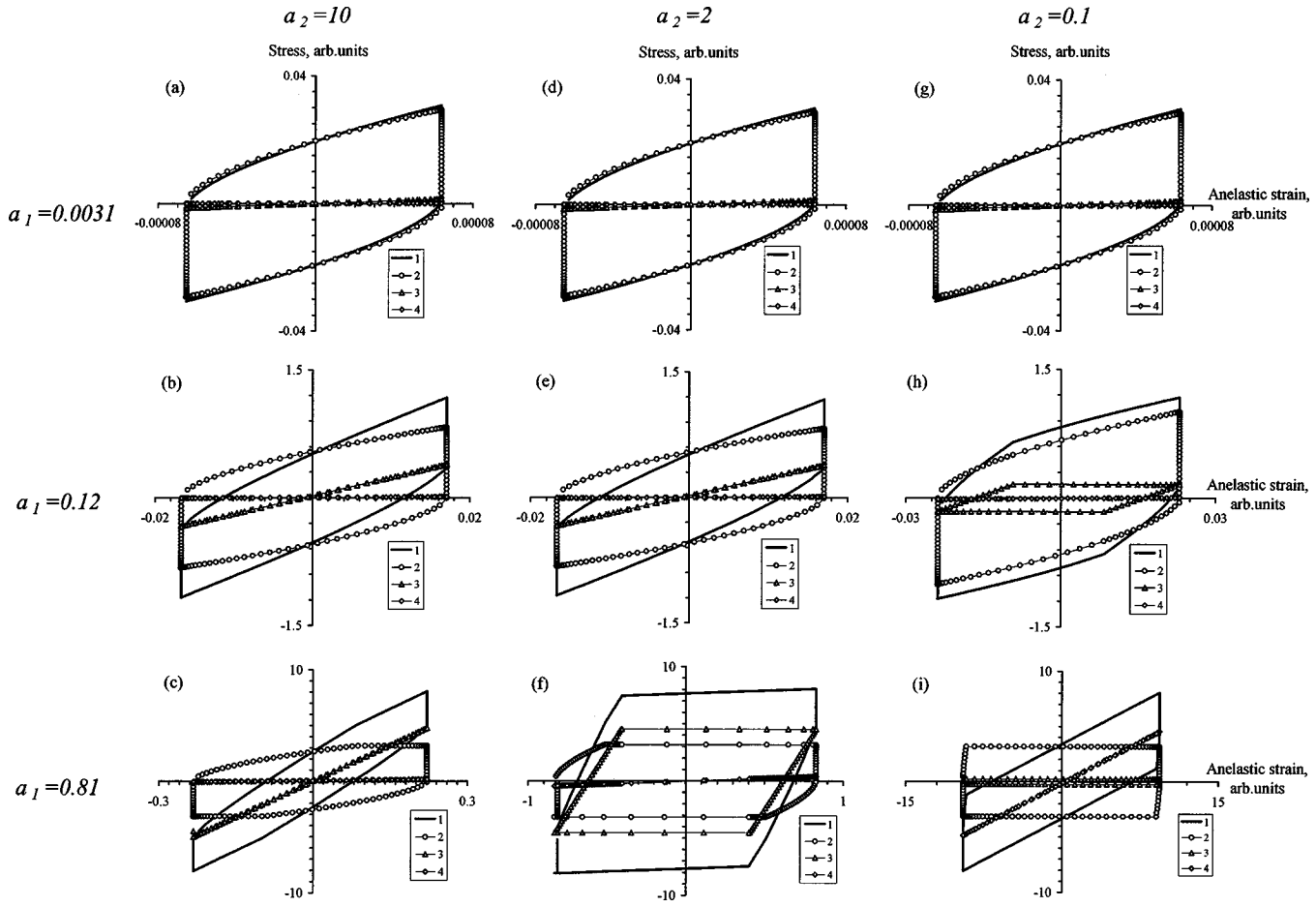

FIG. 7. Calculated total stress-anelastic strain hysteresis loops and their components for the impurity content $C=0.1$ and different values of the parameter a_2 (temperature) and a_1 (stress amplitude): (1) is the total stress-anelastic strain hysteresis; (2) is the hysteresis due to surmounting diffuse localized forces; (3) is the hysteresis due to overcoming localized obstacles; (4) is the line tension between rigid pinners. Model parameters $A_1=15$, $A_2=900$, $A_3=2\times10^{-5}$, $A_4=20$. The hysteresis loops correspond to the data in Fig. 8, where selected stress amplitudes are indicated by the vertical arrows.

$$\delta_h = A_3 \frac{C}{a_1^2} \oint Y d\Sigma,$$

$$\frac{\Delta J}{J} = A_3 \frac{\sqrt{C}}{a_1} Y \Big|_{\sigma=\sigma_0},$$

$$\varepsilon_{\mathrm{an}} = A_4 \sqrt{C} Y. \tag{44}$$

Thus we see from Eq. (44) that the parameters A_3 and A_4 are scaling for the values of the decrement and modulus defect, and anelastic strain, respectively.

Account has also been taken, within each loading cycle, for the strain rate dependence of surmounting localized obstacles by mobile dislocations. As a first approximation we suggested that the critical stress σ_{cr2} is strain-rate dependent

$$\sigma_{\mathrm{cr2}} = \sigma_{\mathrm{cr2}}|_{\dot{\varepsilon}_{\mathrm{an}}=1} (\dot{\varepsilon}_{\mathrm{an}})^{1/m}, \tag{45}$$

where m is a constant parameter. Throughout the present simulations we assumed $m=5$, the value which is representative for the strain rate dependence of the effective stress component during macrodeformation of crystals. Obviously, the parameter m is of secondary importance, since the power dependence in Eq. (45) with the exponent $1/m=0.2$ represent rather weak functions of anelastic strain rate $\dot{\varepsilon}$. Calculations have shown that, indeed, accounting for the strain rate dependence of σ_{cr2} had only a marginal effect on the results.

Numerical integration of Eq. (41) by the Runge-Kutta method was performed using the algorithm from Ref. 20. The technique of calculations was previously designed for determining the nonlinear cyclic anelastic response of solids.[4] Numerical simulation yielded first the dependences $\varepsilon_{\mathrm{an}}(\sigma)$, $\varepsilon_{\mathrm{an}}(\sigma_1)$, $\varepsilon_{\mathrm{an}}(\sigma_2)$, $\varepsilon_{\mathrm{an}}(\sigma_3)$, as is shown, for example, in Fig. 7. From these components of the anelastic response, the values of δ_h, $\Delta J/J$, $r=\delta_h/(\Delta J/J)$, δ_{h1}, $R=\delta_{h1}/\delta_h$ can be easily derived as functions of the dimensionless stress a_1, the temperature-dependent critical stress a_2, and the solute concentration C, where δ_h and δ_{h1} are the total ADIF and its athermal component, respectively, r is the ratio of the ADIF to the amplitude-dependent modulus defect (ADMD), R is the relative fraction of the ADIF due to overcoming of the athermal long-range diffuse forces. The total decrement and its athermal component were calculated from the area within the corresponding hysteresis loops $\varepsilon_{\mathrm{an}}(\sigma)$ and $\varepsilon_{\mathrm{an}}(\sigma_1)$, see Fig. 7. The ADMD was determined as the ratio of the amplitude of the first harmonic component of the anelastic strain in phase with the applied stress to the elastic strain amplitude. Our main concern in the present paper is

the influence of temperature and solute atom content on the strain amplitude dependence of the above-mentioned parameters of nonlinear anelasticity, since they have been reported in a recent detailed experimental study.[9]

A. Model parameters

At the present stage we intend to compare qualitatively the results of simulations with experimental data. Therefore, calculations have been performed for rather arbitrary values of the model parameters. The major part of the calculations has been done for the solute concentration $C=0.1$. The parameter α determines, primarily, the slope of the strain amplitude dependence of the ADIF at low strain amplitudes and is the only one chosen to fit the experimental data. It is associated with the type of dislocation–foreign atom interaction and the distribution of diffuse forces, see Eqs. (20), (21), and (4). Parameters A_1 and A_2, if not specified otherwise, have been set up to 15 and 900, respectively. These parameters are associated, primarily, with the relationship between the retention force due to the diffuse and localized forces, and the line tension due to bowing out between unbreakable obstacles, respectively. For example, the value $A_2=900$ provides $\overline{L/l}=6.5$ for the concentration $C=0.1$. Circular frequency ω was assumed to be 2π. Simulations have been performed assuming homogeneous stress distribution in the crystal. The qualitative comparison will be done with the experimental anelastic behavior under inhomogeneous strain.[9]

B. Results of simulations. Comparison with experiment

1. Influence of temperature on the ADIF, ADMD, and r value

Figure 8 shows the calculated stress amplitude dependence of the ADIF, ADMD, and their ratio r for different values of the parameter a_2. As discussed above, a change of a_2 corresponds to a variation of temperature. Figure 9 represents experimental strain amplitude dependences of the ADIF, ADMD, and the r value, measured in a Cu-7.6 at. % Ni single crystal at a frequency of about 100 kHz, see Ref. 9 for more details. A remarkable qualitative agreement of details of the ADIF, ADMD, and r-value behavior is obtained without fitting of the model parameters.

As has already been intimated,[9] several distinguishing stages of the ADIF behavior with changing the temperature are inherent in solid solutions of fcc metals: (i) Existence of a single athermal low-temperature asymptote with a weak strain amplitude dependence; (ii) Deviation of the ADIF from this asymptote at progressively lower strain amplitudes with increasing temperatures; a pronounced temperature dependence of the ADIF is observed in this stage; (iii) Occurrence of a strongly strain-amplitude-dependent, but weakly temperature-dependent stage with a saturation for the highest strain amplitudes.

The simple microscopic model developed in the present work, shows perfect qualitative agreement with the experimental ADIF behavior. Even more impressive is the agreement of the influence of temperature on the strain amplitude dependence of the ADIF to the ADMD ratio, Figs. 8(c) and 9(c). We note here that, in contrast to the ADIF and ADMD, the calculated r value can be directly compared with the

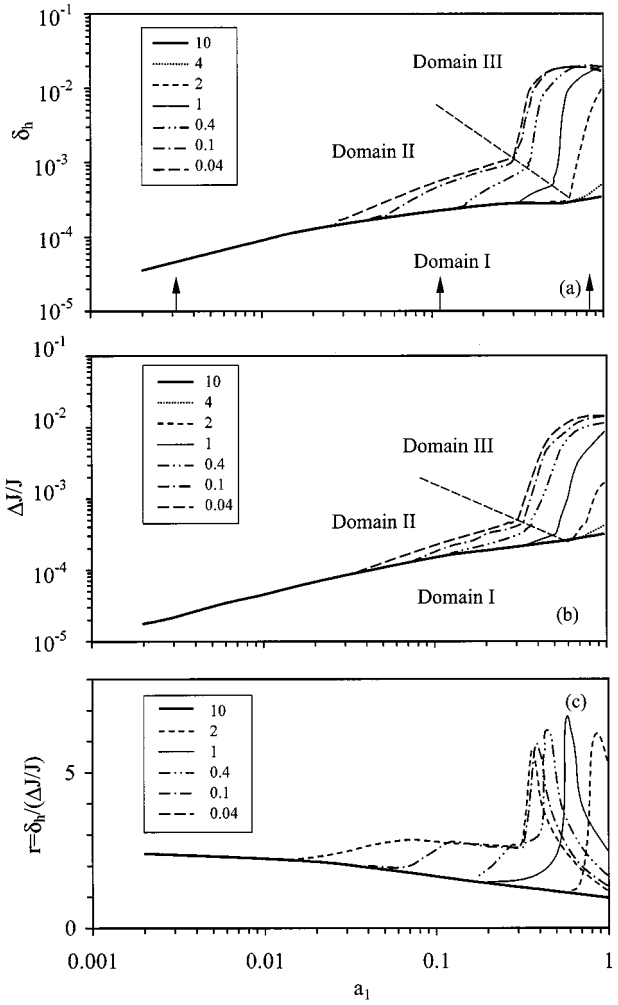

FIG. 8. Calculated stress amplitude dependence of the decrement (a), strain-amplitude-dependent modulus defect (b) and their ratio (c) for impurity content $C=0.1$ at different temperatures (values of the parameter a_2). Model parameters $A_1=15$, $A_2=900$, $A_3=2\times10^{-5}$, $A_4=20$.

experimental results. Numerous details of the $r(\varepsilon_0,T)$ dependences are reproduced in the model: (i) Existence of a low-temperature asymptote, decreasing with the strain amplitude increase from the value $\sim$2.5 to approximately 1; (ii) deviation from this asymptote at progressively lower strain amplitudes with increasing temperature, so as to increase the r value; (iii) Formation of a pronounced maximum of the r value at high strain amplitudes, which shifts to the lower strain amplitudes with increasing temperature.

Ishii[21] was the first to emphasize the importance of the r value to classify mechanisms of the ADIF. He has analyzed a great variety of observed values, as compared with the prediction of the breakaway Granato and Lücke model that the r value is a constant of the order of unity.[22] Up to now, there are few reports on the r-value behavior over a wide range of strain amplitudes.[23,9] See also the analysis of Baker's data[24] in Ref. 21, which show that the r value is essentially not constant. The tradition is still to consider it as a constant parameter, peculiar to a single specific ADIF mechanism.[25] Thus, the present theory enables us to make an attempt to analyze the strain amplitude dependence of the r

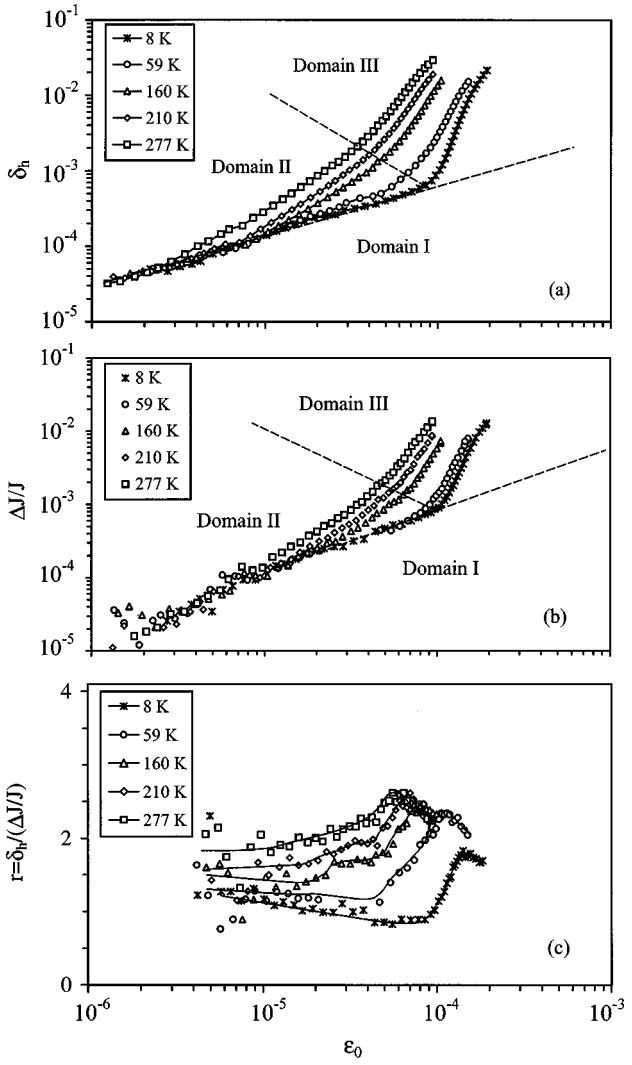

FIG. 9. Experimental strain amplitude dependences of the decrement (a), strain-amplitude-dependent modulus defect (b) and of their ratio (c) for the Cu-7.6 at. % Ni single crystal taken for temperatures 8–277 K at a frequency of about 100 kHz (see Ref. 9 for more results).

value, and a remarkable agreement with experimental results is obtained.

Calculations of the stress-anelastic strain hysteresis allow one to explain peculiarities of the strain-amplitude dependences in Figs. 8 and 9. The hysteresis loops in Fig. 7 correspond to the cross sections of the temperature dependences from Fig. 8, marked off by the arrows. Each vertical column in Fig. 7 represents hysteresis loops at a constant temperature, horizontal row—at a constant stress amplitude.

At low temperatures, Figs. 7(a)–7(c), the anelastic strain is purely hysteretic over the entire range of strain amplitudes. At low and intermediate strain amplitudes, Figs. 7(a) and 7(b), the critical stress σ_{cr1} is not exceeded. Here, the displacement of dislocations is controlled by athermal diffuse forces and line tension between localized obstacles. The stress amplitude dependence of the ADIF and ADMD follows a single low-temperature asymptote in Domain I, see Figs. 8 and 9. The role of the line tension increases with increasing stress amplitude, resulting in the continuous decrease of the r value as depicted in Fig. 8(c). For the highest stress amplitudes, the critical stress σ_{cr1} is exceeded, Fig. 7(c). However, the anelastic strain, ADIF and ADMD do not increase considerably, since the displacement of dislocations is limited by the line tension between localized obstacles.

At intermediate temperatures, Figs. 7(d)–7(f), at low and moderate stress amplitudes, Figs. 7(d) and 7(e), the anelastic behavior is the same as at low temperatures. Therefore, the ADIF and ADMD stress amplitude dependence follows the same low-temperature asymptote in Domain I, Figs. 8 and 9. However, localized forces can now be surmounted at high stress amplitudes. When both critical stresses are exceeded, a drastic increase of the anelastic strain occurs, Fig. 7(f), since the strain becomes controlled only by the line tension between unbreakable obstacles. Therefore, the steep rise of the ADIF and ADMD is observed when both critical stresses are exceeded in Domain III, Figs. 8 and 9.

For the range of high temperatures, the critical stress for the motion over localized obstacles becomes low and can be exceeded at moderate stress amplitudes, Fig. 7(h). This leads to a deviation of the ADIF and ADMD from the low-temperature asymptote and the formation of a weakly stress-amplitude-dependent, but strongly temperature-dependent trend in Domain II. Exceeding of the critical stress σ_{cr2} is not accompanied by a steep rise of the anelastic strain [ADIF and ADMD, see Figs. 8(a) and 8(b)], since the diffuse forces limit dislocation displacement. A pronounced increase of the anelastic strain occurs only when the temperature-independent critical stress σ_{cr1} is also exceeded at higher stress amplitudes, Fig. 7(i).

2. Influence of substitutional atom concentration on the ADIF

Figure 10(a) depicts the calculated strain amplitude dependence of the ADIF for different solute concentrations C. The range of concentrations used corresponds to the variation of the ratio $\overline{L}/\overline{l}$ from 1.4 to 10.5 for the concentrations of 0.01 and 0.2, respectively. Thus, the simulation appears to be meaningless for lower concentrations, having the fixed value of the restoring force due to the line tension between unbreakable obstacles [parameter S, see Eq. (30)], since it becomes lower than the restoring force due to the line tension between localized forces. For lower C, one should decrease the S parameter as well. This requirement is in fair agreement with the well-known increase of the dislocation density in deformed crystals with the impurity content. For example, the dislocation pattern in the CuNi system changes from a homogeneous distribution for Cu-2 at. % Ni to a more heterogeneous one with high dislocation density in slip lines for Cu-5 at. % Ni crystals.[26,27] Figure 10(b) represents the experimental strain amplitude dependence of the decrement for crystals of the CuNi system, taken at low temperature (more data can be found in Ref. 9). Again, a remarkable agreement is observed about the details of the experimental and calculated results in a qualitative, if not almost quantitative, manner:

(i) an increase of the low-temperature and low-amplitude ADIF without change of the slope of the stress amplitude dependence,

(ii) a shift of the strongly strain-amplitude-dependent stage of the ADIF to higher stress amplitudes with the increase of impurity content,

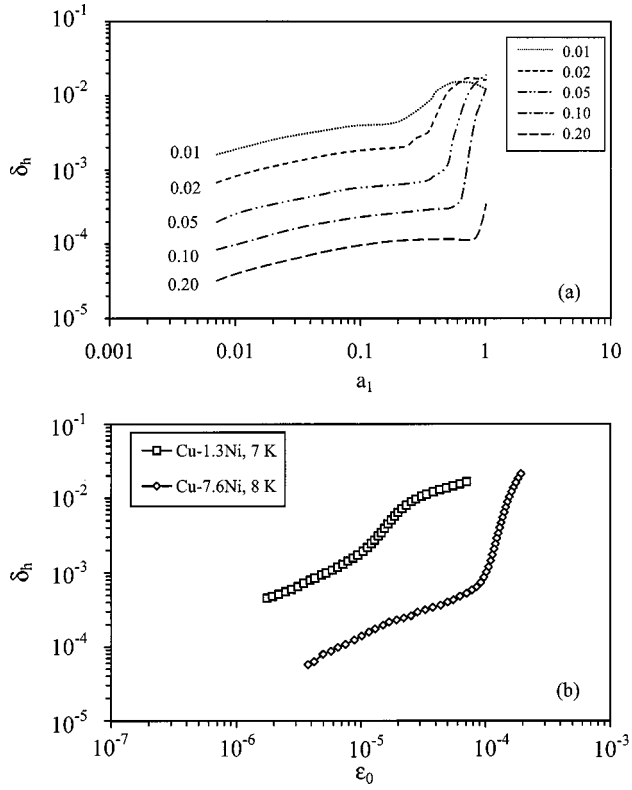

FIG. 10. Influence of the impurity content on the amplitude dependence of the internal friction: (a) calculated stress amplitude dependences for different impurity contents and $a_2=2$; model parameters $A_1=15$, $A_2=900$, $A_3=2\times10^{-5}$, $A_4=20$; (b) experimental strain amplitude dependences for Cu-1.3 at. % Ni and Cu-7.6 at. % Ni crystals, measured at low temperatures at a frequency of about 100 kHz (see Ref. 9 for more details).

(iii) an increase of the slope of the steep ADIF stage for higher impurity concentration,

(iv) more (low impurity content) or less (high concentration of impurity) pronounced saturation of the ADIF stress amplitude dependence for the highest stress amplitudes.

It is worthwhile to note here that the model predicts the existence of a peaking effect as a function of the solute atom (or irradiation defect) content. Indeed, for $C=0$ the ADIF becomes zero, since only the line tension between unbreakable obstacles controls dislocation motion. Thus, the decrease of the ADIF with solute concentration at higher C, see Fig. 10, implies the existence of a maximum as a function of the impurity (or irradiation defect) contents, that is, the peaking effect.

3. Athermal and thermally activated components of strain-amplitude-dependent internal friction

In this section we will analyze stress amplitude–temperature dependence of the relative fraction of the ADIF due to athermal events, $R=\delta_{hl}/\delta_h$, i.e., the ADIF fraction due to the dislocation overcoming diffuse forces. The results of the calculations are depicted in Fig. 11. The fraction of the total damping due to the athermal diffuse forces is represented for the stress amplitude dependences of the decrement at different values of the a_2 parameter (different temperatures) from Fig. 8(a). As one may expect, the contribution of

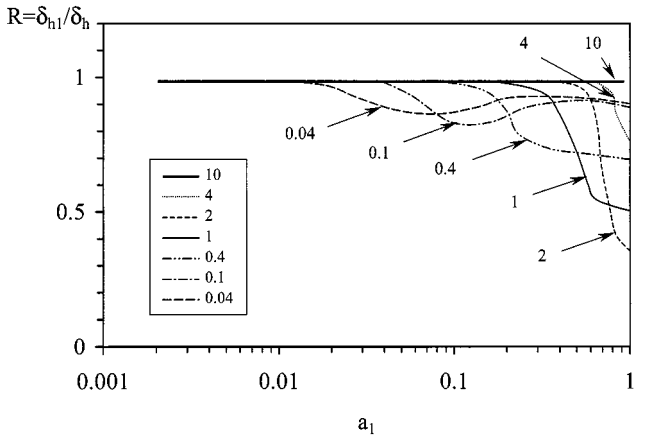

FIG. 11. Stress amplitude dependence of the fraction of the athermal damping, calculated for different temperatures (values of a_2). The results correspond to the data in Figs. 7 and 8(a).

the athermal events approaches 1 at very low and becomes smaller at very high temperatures, that is the contribution of the thermally activated events exhibits a maximum as a function of temperature. R also exhibits a maximum on the stress amplitude scale. The position of this maximum shifts to lower stress amplitudes when the temperature is increased. A remarkable result is that in a large part of the stress-temperature domain, the contribution of the athermal events is overwhelming. In only a relatively narrow range of temperatures and stress amplitudes is the contribution of thermally activated overcoming of localized forces higher than that of the athermal surmounting the diffuse forces (R is lower than 0.5).

Quite interesting are certain details of the decrement and R behavior in Domain II, see Fig. 8(a). At a first glance, one might expect the increase of the decrement in this domain after exceeding σ_{cr2} be due to the overcoming localized forces. A straightforward way to estimate the contribution of the thermally activated events would be to subtract the values of the decrement at the low-temperature asymptote from the current values, as it is usually done for the strain-amplitude-dependent and independent IF components. This simple operation would result in a predominant contribution of the thermally activated component, since the decrement increases up to 3 to 4 times in Domain II, as compared with the low-temperature asymptote, see Fig. 8(a). However, this straightforward approach gives completely wrong results and the real contribution of the thermally activated events remains relatively low, see Fig. 11. The reason for that is the fact that thermally activated and athermal events are interrelated via the anelastic strain amplitude. A deviation from the low-temperature asymptote implies an increase of the anelastic strain amplitude in Domain II [ADMD, see Fig. 8(b)], and, as a consequence, an increase also of the athermal ADIF component, as compared with the low-temperature asymptote.

Thus we conclude that, in the major part of the temperature-stress amplitude domain, the ADIF is predominantly due to the motion over athermal diffuse forces, despite the pronounced temperature dependence of the ADIF, for example, in Domain II.

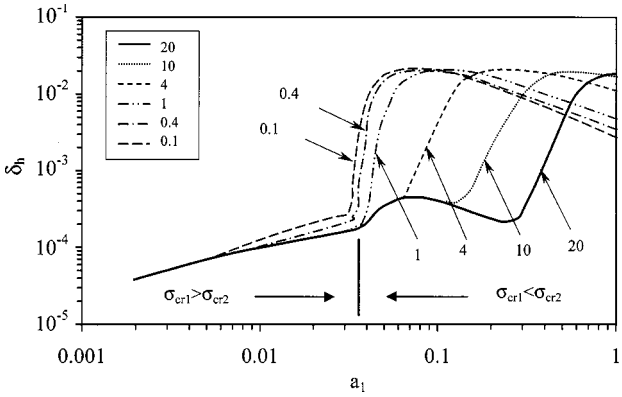

FIG. 12. Calculated stress amplitude dependence of the decrement for solute atom concentration $C=0.1$ and different temperatures (values of the parameter a_2), showing the influence of the relationship between critical stresses σ_{cr1} and σ_{cr2} on the expected temperature dependence of the decrement. Values of model parameters: $A_1=36$, $A_2=900$, $A_3=2\times10^{-5}$, $A_4=2$.

C. Critical stresses for dislocation motion over diffuse and localized forces

An essential assumption underlying the results reported in previous sections is that the critical stress for the motion of dislocations over diffuse forces can be higher than the critical stress related to their motion over the localized ones. Before analyzing the situation in more detail, we shall first present the results of the simulations in a wide range of critical stress σ_{cr2} (temperatures), when σ_{cr2} is both significantly higher or lower than σ_{cr1}. Figure 12 demonstrates such results. The critical stress σ_{cr1} has been decreased an order of magnitude, as compared to the results in Figs. 7, 8, and 10. The vertical line in Fig. 12 separates approximately the domains with different relationship between σ_{cr1} and σ_{cr2}. Strictly speaking, there is no fixed value of the applied stress dividing these domains, since σ_{cr2} is not constant for each of the strain amplitude dependences, but depends slightly on the strain rate (stress amplitude). Nevertheless, such an approximate division of the domains is representative. Obviously, the ADIF behavior is essentially the same at low stress amplitudes (Domain I), when neither of the critical stresses is exceeded. At higher stress amplitudes, the ADIF behavior shows a perfect at the very least qualitative agreement with experimental results when $\sigma_{cr1}>\sigma_{cr2}$. In contrast, the ADIF behavior diverges fundamentally from the experimental data when $\sigma_{cr2}>\sigma_{cr1}$: After exceeding the critical stress σ_{cr1}, the ADIF deviates from the low-temperature and low-strain amplitude asymptote; however, this deviation is purely temperature independent. A transition to a steep stage of the ADIF, on the contrary, is strongly temperature dependent.

Thus, good agreement of the suggested model with numerous experimental observations, assuming that σ_{cr1} can be lower than σ_{cr2} and a radical discrepancy otherwise, enables us to conclude that diffuse forces exerted on a mobile dislocation in a solid solution, at least at elevated temperatures, can be predominant over the localized ones. To justify this statement, we would like to point here to an issue apparently missing in the previous works. The assertion that localized forces are always predominant over the diffuse ones is based on the analysis performed by Nabarro[13] and Labusch.[28] However, Nabarro made the estimations for the flow stress at $T=0$ K. Labusch[28] also did not consider the influence of temperature on the diffuse and localized forces. We believe that generalization of this conclusion to the range of elevated temperatures is not justified if diffuse forces represent long-range elastic stress fields, which are surmounted athermally. Indeed, the critical stress for the motion over diffuse forces is temperature independent, whereas the critical stress of motion over localized obstacles is strongly reduced with increasing temperature. Therefore, it appears quite plausible that, at elevated temperatures, diffuse forces may become predominant over the localized ones. This statement also follows directly from Friedel's conclusion that the long-range hardening by solute atoms is responsible, at least partly, for the athermal high-temperature plateau of the elastic limit of solid solutions.[14]

IV. CONCLUSION

The suggested microscopic model for the dislocation-solute atom interactions in solid solutions enabled us to calculate the nonlinear dislocation anelasticity in solid solutions. A complicated multistage behavior of the internal friction, Young's modulus defect, and their ratio in the temperature–strain amplitude–solute concentration domain is predicted. Results of numerical simulations show good, at the very least qualitative, agreement with experimental data. The agreement implies that, as opposed to the conventional approach, the critical stress for the motion of dislocations in the field of diffuse forces due to foreign atoms situated away from the dislocation glide plane may exceed the critical stress due to localized interactions with foreign atoms in a few atomic planes adjacent to the dislocation glide plane.

ACKNOWLEDGMENTS

The support of this work by the Swiss National Science Foundation through Project No. 7 IP 051832.97/1 is gratefully acknowledged.

*Permanent address: A. F. Ioffe Physico-Technical Institute, Politeknicheskaya, 26, 194021 St. Petersburg, Russia.

[1] A. S. Nowick and B. S. Berry, *Anelastic Relaxation in Crystalline Solids* (Academic, New York, 1972).

[2] G. Fantozzi, C. Esnouf, W. Benoit, and I. G. Ritchie, Prog. Mater. Sci. **27**, 311 (1982).

[3] J. Dralla and J. C. Bilello, J. Appl. Phys. **41**, 2340 (1970); D. G. Pinatti and J. M. Roberts, *ibid.* **53**, 933 (1982); J. M. Roberts, Phys. Status Solidi A **19**, 731 (1973); **20**, 145 (1973); S. Kustov and S. Golyandin, ASTM STP N 1304, 1997, p. 22 (unpublished).

[4] S. N. Golyandin and S. B. Kustov, Fiz. Tverd. Tela (Leningrad) **34**, 3796 (1992) [Sov. Phys. Solid State **34**, 2031 (1992)]; **34**, 3804 (1992) [**34**, 2035 (1992)].

[5] G. Gremaud, J. Phys. (Paris), Colloq. **48**, C8-15 (1985).

[6] J. Baur and W. Benoit, J. Appl. Phys. **60**, 3473 (1986); **61**, 2463 (1987); J. Baur, M. Bujard, and W. Benoit, J. Phys. (Paris), Colloq. **46**, C10-239 (1985).

[7] H. M. Simpson, A. Sosin, and D. F. Johnson, Phys. Rev. B **5**, 1393 (1972); C. Minier, J. Lauzier, C. Esnouf, and G. Fantozzi, J. Phys. (Paris), Colloq. **44**, C9-51 (1983).
[8] S. B. Kustov, S. N. Golyandin, I. Hurtado, J. Van Humbeeck, and R. De Batist, J. Phys. IV **6**, C8-389 (1996); S. Kustov, S. Golyandin, K. Sapozhnikov, J. Van Humbeeck, and R. De Batist, Acta Mater. **46**, 5117 (1998).
[9] S. Kustov, G. Gremaud, W. Benoit, S. Golyandin, K. Sapozhnikov, Y. Nishino, and S. Asano, J. Appl. Phys. **85**, 1444 (1999).
[10] U. F. Kocks, A. S. Argon, and M. F. Ashby, *Thermodynamics and Kinetics of Slip* (Pergamon, New York, 1975), p. 160; J. Ni and J. Schlipf, in *Proceedings of The 9th International Conference on Internal Friction and Ultrasonic Attenuation in Solids*, Beijing, China, 1989, edited by T. S. Kê (IAP, Pergamon, Oxford, 1990), p. 53.
[11] P. Haasen, in *Dislocations in Solids*, edited by F. R. N. Nabarro (North-Holland, Amsterdam, 1979), Vol. 4, Chap. 15, p. 155.
[12] It is shown in Sec. III A that in the present theory the nature of dislocation–foreign atom interaction influences only certain numerical parameters, leaving the general conclusions of the theory essentially the same.
[13] F. R. N. Nabarro, in *The Physics of Metals*, edited by P. B. Hirsch (Cambridge University Press, Cambridge, 1975), Vol. 2, Chap. 4, p. 152.
[14] J. Friedel, in *Proceedings of the National Physical Laboratory Conference on the Strength of Alloys*, 1963 (Pergamon, London, 1964), Vol. 1, p. 410.
[15] G. Gremaud and S. Kustov (unpublished).
[16] R. Schindlmayr and J. Schlipf, Philos. Mag. **31**, 13 (1975).
[17] U. F. Kocks, A. S. Argon, and M. F. Ashby, *Thermodynamics and Kinetics of Slip* (Ref. 10), p. 53.
[18] See Kocks, Argon, and Ashby (Ref. 17), p. 58.
[19] R. B. Schwarz and R. Labusch, J. Appl. Phys. **49**, 5174 (1978); Kocks, Argon, and Ashby (Ref. 17), p. 110; J. Schlipf, Phys. Status Solidi A **74**, 529 (1982).
[20] G. E. Forsythe, M. A. Malcolm, and C. B. Moler, *Computer Methods for Mathematical Computations* (Prentice-Hall, Englewood Cliffs, NJ, 1997).
[21] K. Ishii, J. Phys. Soc. Jpn. **52**, 141 (1983).
[22] A. V. Granato and K. Lücke, J. Appl. Phys. **27**, 583 (1956).
[23] V. Ya. Platkov and I. K. Nosolev, Izv. Ross. Akad. Nauk, Ser. Fiz. **57**, 26 (1993) (in Russian); K. V. Sapozhnikov, S. N. Golyandin, S. B. Kustov, Y. Nishino, and S. Asano, Philos. Mag. A **77**, 151 (1998).
[24] G. S. Baker, J. Appl. Phys. **28**, 734 (1957).
[25] A. B. Lebedev, J. Phys. IV **6**, C8-325 (1996).
[26] H. Neuhäuser and O. B. Arkan, Phys. Status Solidi A **100**, 441 (1987).
[27] S. N. Golyandin and S. B. Kustov, Fiz. Tverd. Tela (St. Petersburg) **37**, 3248 (1995) [Phys. Solid State **37**, 1786 (1995)].
[28] R. Labusch, Phys. Status Solidi **41**, 659 (1970).